Hindawi
Advances in Condensed Matter Physics
Volume 2022, Article ID 2450578, 7 pages
https://doi.org/10.1155/2022/2450578

Research Article

Electric Modulus Analysis of $(1-x)$ $PbMg_{1/3}Nb_{2/3}O_3$-(x) $K_{1/2}Bi_{1/2}TiO_3$ Ceramics

Kebede Legesse, Vijaya Bhaskar Rao Poluri, and Elangovan Sampandam

Department of Physics, College of Natural and Computational Sciences, Wollega University, Nekemte, Ethiopia

Correspondence should be addressed to Kebede Legesse; kebedelegesse@gmail.com

Received 4 January 2022; Accepted 28 February 2022; Published 22 March 2022

Academic Editor: Ram N. P. Choudhary

Ferroelectrics refer to groups of dielectrics having the property of spontaneous polarization. Lead magnesium niobate-potassium bismuth titanate ($(1-x)$ $PbMg_{1/3}Nb_{2/3}O_3$-$(x)K_{1/2}Bi_{1/2}TiO_3$)) $x=0.15$, 0.25, and 0.35 are prepared by solid-state reaction rout technique. The electric modulus of the prepared samples is studied using the complex impedance spectroscopic method at 400°C, 450°C, and 500°C in various frequency ranges. In the lower frequency range, the real modulus (M' (ω)) decreased with increasing the temperature. Furthermore, the real modulus (M' (ω)) increased with increasing frequency and the concentration of the doping component. The imaginary modulus (M'' (ω)) increased with increasing the temperature. The significant variations in the real and imaginary coefficients signify the existence of thermally activated dielectric relaxation between the selected components. Moreover, the magnitude of grain capacitance increased with increasing the temperature, confirming the negative temperature coefficient of resistance of the material.

1. Introduction

Ferroelectric ceramics with the structure of ABO_3 (perovskite) have taken a vital role in the production of fuel cells. Relaxor ferroelectric ceramics with perovskite structures can be used as transducers, actuators, and sensors [1–3]. Since lead magnesium niobate and potassium bismuth titanate are ferroelectric materials, they possess volatile electrical properties. ($PbMg_{1/3}Nb_{2/3}O_3$) (PMN) is a B-site complex perovskite relaxor ferroelectric material that has a broad and high frequency-dependent of permittivity peak as the function temperature. The sharp and lower peaks of normal ferroelectric material which follow the phase transition of the Curie–Weiss law is different from that of the relaxor ferroelectric properties. ($PbMg_{1/3}Nb_{2/3}O_3$) (PMN) has a diffused phase and maximum dielectric constant obtained at −10°C [4, 5]. Lead magnesium niobate (PMN) ferroelectric relaxors exhibit desirable dielectric properties, low loss, a wide dielectric peak, nonhysteric behavior, and low sintering temperature. However, there are some disadvantages to PMN such as low electromechanical coupling, toxicity due to the presence of lead in it, and low working temperature. Hence, some other lead-reduced or lead-free relaxor ferroelectric materials are needed. The toxicity of lead oxide during the preparation of PMN is one cause for a search for new alternative lead-reduced materials. Mixing another ferroelectric material with ($PbMg_{1/3}Nb_{2/3}O_3$) (PMN) while using the solid-state reaction route increase the stability of sample formation in which pyrochlore phases-free perovskite structure may form than preparing pure PMN.

The dielectric properties of relaxor ferroelectric PMN can be enhanced by the addition of ferroelectric materials such as $PbTiO_3$ (PT) and lead zirconate titanate ($PbZr_xTi_{1-x}O_3$) (PZT), but the problem behind these materials is that these are composed of lead oxide which is toxic material [6]. Considerations connected with the protection of the environment and the health of the world's population stimulate intensive research of new alternative FE materials which would not contain lead or would contain it only in small concentrations. Potassium bismuth titanate ($K_{1/2}$ $Bi_{1/2}$) TiO_3 (KBT) is an attractive example of lead-free A-site complex

ferroelectric material [7]. Potassium bismuth titanate ($K_{1/2}Bi_{1/2}$)TiO_3 (KBT) has a broad frequency-dependent high peak at a temperature of 380°C and exhibit relaxor property [8]. It is lead-free perovskite ceramic so it is one of the environment-friendly materials. However, there are also some shortcomings to KBT as well. These properties are still notably inferior to that of lead-based ones, for instance, in its electrical properties, it has a low dielectric constant (ε_r) [9]. It has a high Curie temperature (T_c) which results in being unsuitable for working at low temperatures. It is realistic that we need the Curie temperature to be near to room temperature for many applications, hence reducing the Curie temperature (T_c) for potassium bismuth titanate ($K_{1/2}Bi_{1/2}$) TiO_3 increases its advantages [10]. Impedance and modulus properties of PMN-KBT are important for investigating the viability of PMN-KBT relaxor ferroelectric materials for sensor and actuator applications. No studies are reported on lead magnesium niobate -potassium bismuth titanate ceramic systems. This study is an attempt to elucidate the modulus property of $((1-x)$ $PbMg_{1/3}Nb_{2/3}O_3$-$(x)K_{1/2}Bi_{1/2}TiO_3$) ceramic with $x = 0.15$, 0.25, and 0.35 using the CIS technique.

$PbMg_{1/3}Nb_{2/3}O_3$ and $K_{1/2}Bi_{1/2}TiO_3$ exhibit desirable dielectric properties and also promising potential for lead-free ferroelectric materials. The lead-based relaxer ferroelectric such as PMN is widely used in various applications but highly toxic. Furthermore, lead-free relaxor such as KBT in their practical application and their performance at the device level is yet to be established. Hence, this work is an attempt to study the electric modulus analysis of $(1-x)$ $PbMg_{1/3}Nb_{2/3}O_3$-$(x)K_{1/2}Bi_{1/2}TiO_3$ ceramics in detail the structural and electrical properties of $(1-x)$ $PbMg_{1/3}Nb_{2/3}O_3$-$(x)K_{1/2}Bi_{1/2}TiO_3$ solid solution with $x = 0.15$, 0.25, and 0.35.

2. Experimental Procedures

$(1-x)$ $(PbMg_{1/3}Nb_{2/3}O_3)$-$(x)K_{1/2}Bi_{1/2}TiO_3$ ceramics with $x = 0.15$, 0.25, and 0.35 were synthesized using the solid-state reaction method. PbO, MgO, Nb_2O_5, K_2CO_3, Bi_2O_3, and TiO_2 (purity 99.9%) were used as raw materials. Lead magnesium niobate ($PbMg_{1/3}Nb_{2/3}O_3$) (PMN) powder was prepared through the columbite route [11]. According to the columbite route, the stoichiometric amount of MgO and Nb_2O_5 were taken and mixed with acetone as a mixing medium, and then using an agate mortar and pestle the powder was ground for six hours. To form columbite powder ($MgNb_2O_3$), a ground mixture was calcined for six hours at a temperature of 800°C in a furnace. Lead mono oxide (PbO) was mixed with the prepared columbite powder ($MgNb_2O_3$) using an agate mortar and pestle according to their stoichiometric ratio to form a nanopowder of lead magnesium niobate ($PbMg_{1/3}Nb_{2/3}O_3$) (PMN). This powder was for four hours calcined in a crucible at 800°C and then, using the X-ray diffractometer, checked the phase purity. KBT powder was prepared, similarly through a solid-state reaction route from starting powders, K_2CO_3, Bi_2O_3, and TiO_2. The stoichiometric amount of these powders was mixed using acetone as mixing media and then, using an agate mortar and pestle, it was grounded for six hours. At the temperature of 800°C, the mixture was dried and calcined in alumina crucibles to obtain fine powder and then checked for phase formation using the X-ray diffractometer.

After the preparation of the main precursors, PMN and KBT, $(1-x)$ $(Mg_{1/3}Nb_{2/3})O_3$-$(x)K_{1/2}Bi_{1/2}TiO_3$ ceramic systems were prepared from these precursors. A stoichiometric amount of PMN and KBT powders were mixed with acetone using an agate mortar and pestle to form a fine powder of lead magnesium niobate ($PbMg_{1/3}Nb_{2/3}O_3$) (PMN)-potassium bismuth titanate ($K_{1/2}Bi_{1/2}TiO_3$) (KBT). This powder was calcined for 4 hrs in a crucible at 800°C. The calcined powders were mixed with polyvinyl alcohol (PVA) which helps as a binder in reducing the brittleness of the pellet. Furthermore, the PVA burnt out during the sintering process. Then, to have cylindrical pellets of 10 mm diameter and 1.5 mm thickness, the samples were pressed using a hydraulic press under a load of 12.5 kN. At a temperature of 1000°C for four hours, the pellets were sintered. The flat surfaces were polished, and electrodes with a silver paste were dried under a lamp for thirty minutes to remove moisture for the electrical measurement. Finally, in the wide temperature (25–500°C) and frequency range (100 Hz–1 MHz) by the CIS-techniques, the researchers recorded the data.

3. Theory

Various parameters are calculated by using the standard relations which are reported in the available literature [12–15].

$$M^* = M' + jM'', \tag{1}$$

$$M^* = j\omega\varepsilon_0 Z^*, \tag{2}$$

where M' is the real part of electric modulus and M'' imaginary part of electric modus.

For the parallel combination of RC elements, the link between impedance and modulus showing the real and imaginary part of the modulus are given by

$$M\prime = \omega\varepsilon_0 Z\prime\prime, \tag{3}$$

$$Z\prime\prime = \frac{\omega CR^2}{1+(\omega CR)^2}, \tag{4}$$

$$M\prime = \frac{C\varepsilon_0\omega^2 R^2}{1+(\omega CR)^2}, \tag{5}$$

$$M\prime\prime = \omega\varepsilon_0 Z\prime, \tag{6}$$

$$Z\prime = \frac{R}{1+(\omega CR)^2}, \tag{7}$$

$$M\prime\prime = \frac{\varepsilon_0\omega R}{1+(\omega CR)^2}, \tag{8}$$

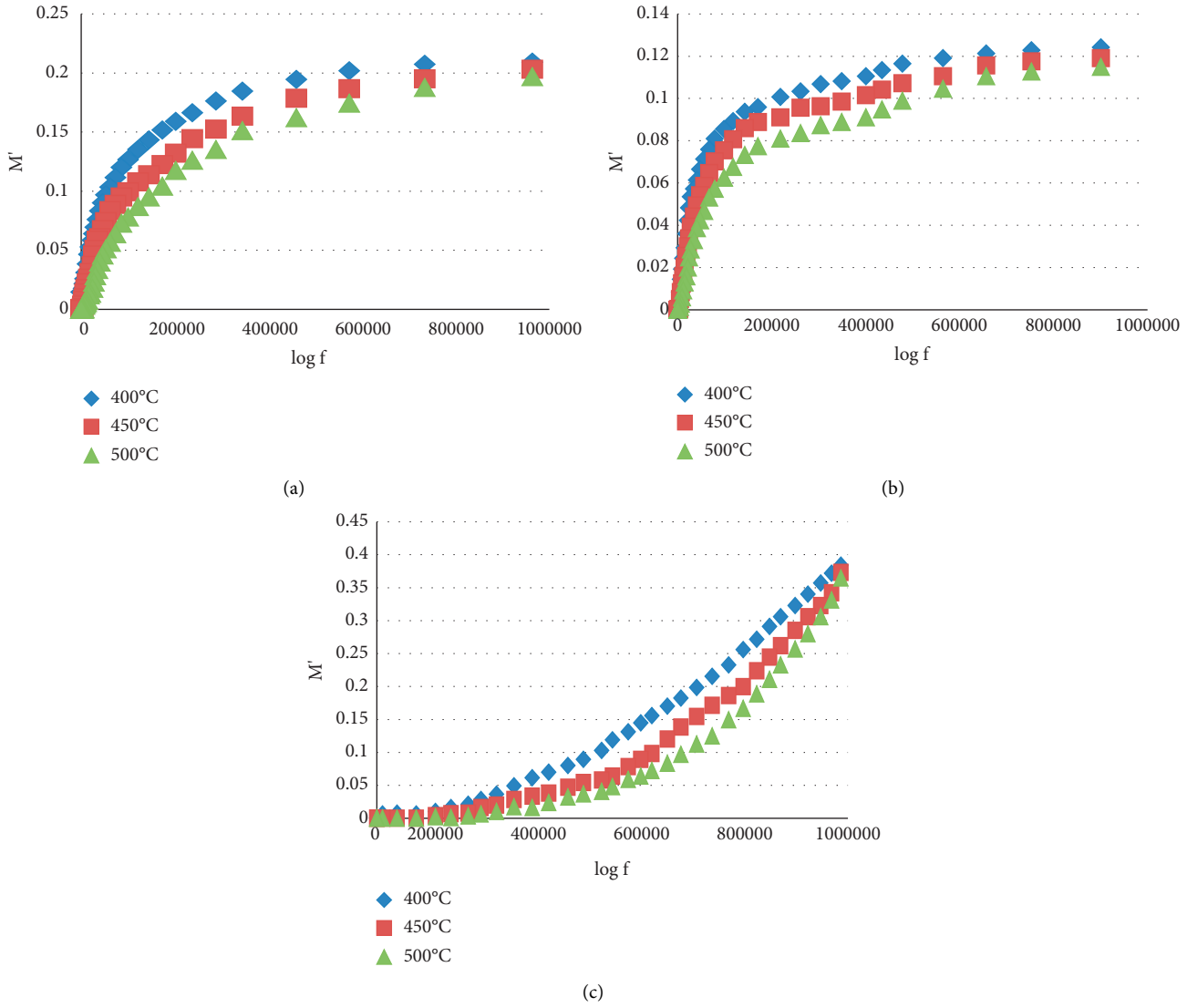

Figure 1: M' versus frequency for (a) 0.85PMN-0.15KBT, (b) 0.75PMN-0.25KBT, and (c) 0.65PMN-0.35KBT compositions at different temperatures.

$$\varepsilon = \frac{C_g}{C_0}, \tag{9}$$

$$C_0 = \frac{\varepsilon_0 A}{t}, \tag{10}$$

$$C_g = \frac{\varepsilon\varepsilon_0 A}{t}, \tag{11}$$

where A is the area and t is the thickness of the sample.

M' versus frequency at different temperatures is shown in Figures 1(a)–1(c) for $(1-x)$PMN-xKBT ($x = 0.15$, 0.25, and 0.35). Only the grain effect is seen by the real modulus (M') method being due to their huge values the layer effect is suppressed.

4. Results and Discussion

The role of different parts of the materials such as the effect of the electrode, bulk, interfaces, and grain boundary can be determined through an impedance spectroscope. The complex permittivity (ε^*), complex impedance (Z^*), complex admittance (Y^*), and complex modulus (M^*) were determined at various temperatures and frequency ranges. The complex electric modulus (M^* (ω)) can be used to analyze the dielectric properties of materials [16–19]. The electrical relaxation of the conducting materials can be studied by modulus spectroscope which is useful to suppress electrode effect [20]. The dielectric properties can be rationalized by the combined usage of impedance and modulus spectroscopic plots. The main advantage of modulus plots is that it is used to measure elements with the smallest capacitance and M'' versus M' plot is used to highlight the smallest capacitive element.

In the lower frequency range, the temperature increases result in the decrease of the real modulus (M′ (ω)) but increase its value at higher frequencies as shown in Figures 1(a)–1(c). The value of the real modulus (M′ (ω)) comes close to zero because the electrode effects are

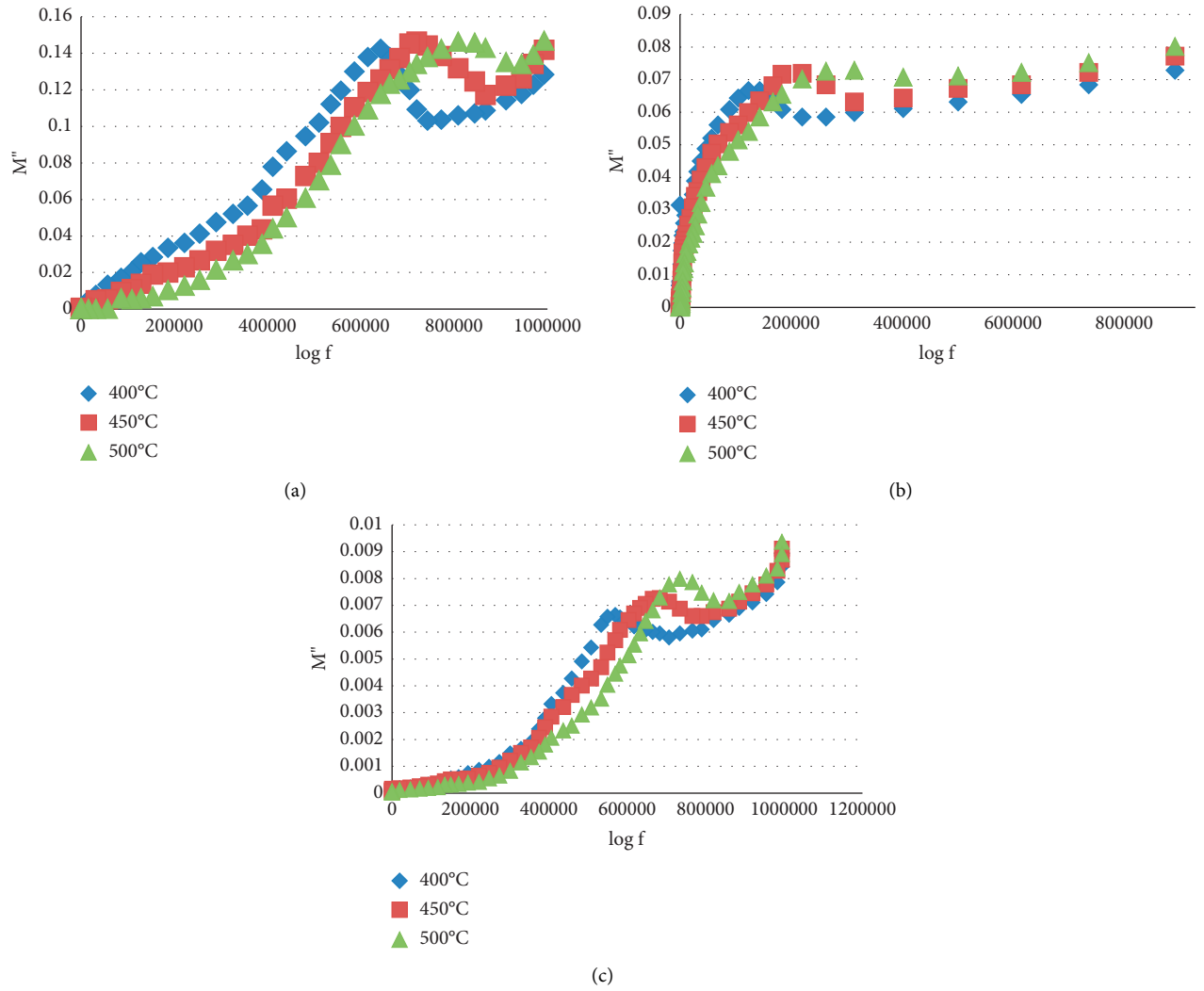

FIGURE 2: M'' versus frequency for (a) 0.85PMN-0.15KBT, (b) 0.75PMN-0.25KBT, and (c) 0.65PMN-0.35KBT compositions at different temperatures.

dominant at low frequencies. At lower temperatures, the space charge accumulates so that the electrode polarization contribution takes a vital role at the interface, but the interface effects are getting rid of in the modulus depiction [21].

At various measuring temperatures, the dependence of M″ on the frequencies is shown Figures 2(a)–2(c). Under the applied electrical field the energy loss implies the imaginary part of electrical modulus. In the modulus analysis, the value of $M''(\omega)$ is very small at lower frequency showing that the effect of the electrode is negligible so that it can be ignored. As the frequency increase, the value of the imaginary modulus $M''(\omega)$ increases as it is noticed in the figure and there is a slight peak position shift towards the higher frequencies as temperature increases. This indicates thermally activated dielectric relaxation in which the main process of charge carrier is the hopping process [22]. In the real ionic conductors also this type of modulus spectra has been observed. In the M'' versus frequency plot, the transition from the long-range to the short-range mobility is indicated by the region the peak occurs with an increase in frequency [23]. Long-range hopping takes place in frequency regions below the peak maximum and short-range hopping takes place because the charge carriers are confined to the potential well. So, the observations signify the existence of a temperature-dependent hopping type of charge transport. As it is seen from Figure 2 the broadening of the peak is an indication of the spread of the relaxation with the distribution of relaxation time constant. In addition, the presence of real dielectric relaxation is shown by the appearance of the peaks in the M″ versus frequency plot [24]. At high frequencies, M' and M'' increase and reach their maximum values with the increasing temperatures. These values show the shortage of force that governs the mobility of charge carriers (restoring force) under the action of the induced electric field. The absence of electrode polarization may be a cause for the low value of M'' observed at lower frequencies. Figures 2(a)–2(c) also clearly show that as the value of the composition (x) increase, the magnitude of M'' decrease.

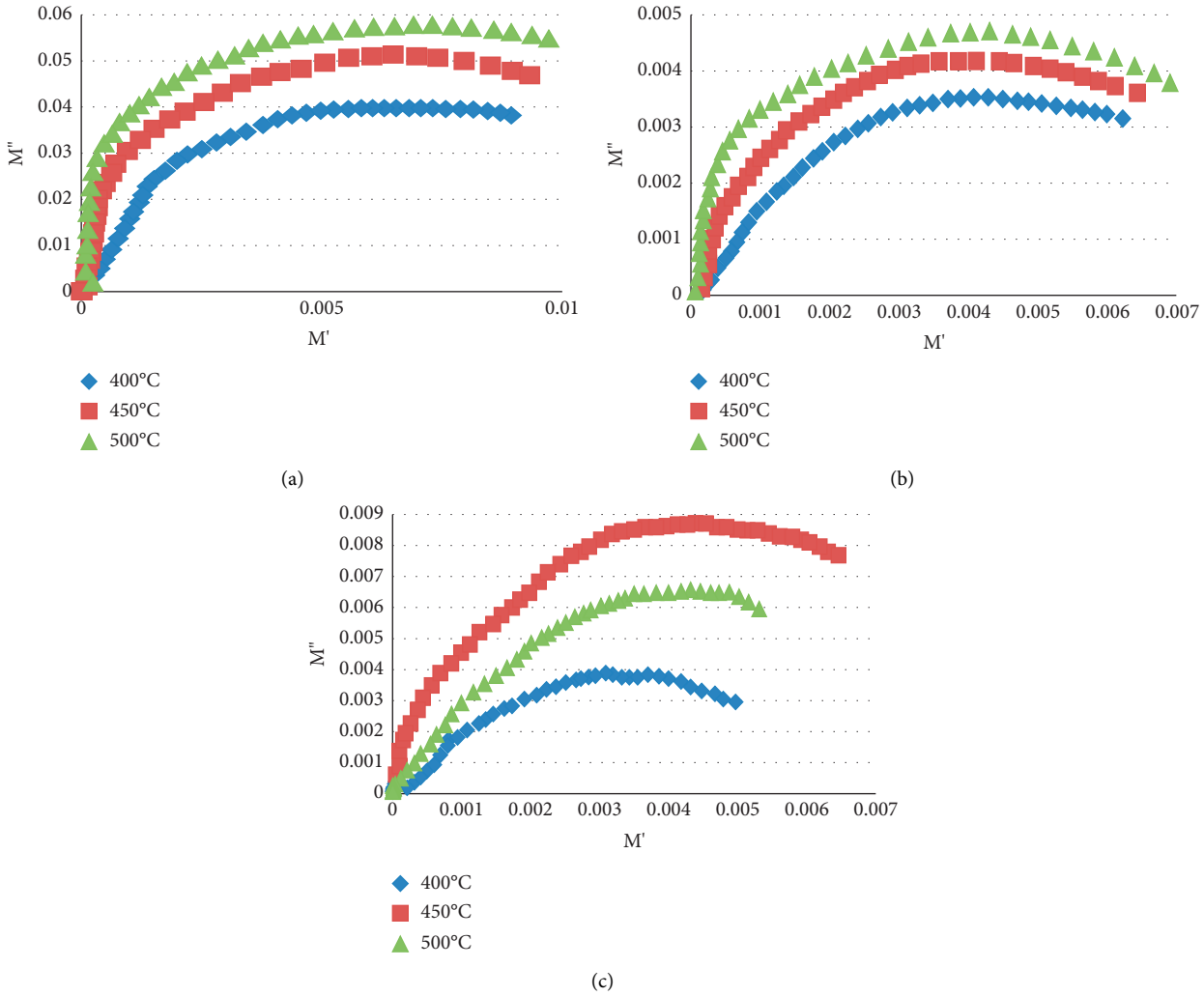

FIGURE 3: M' versus M'' for (a) 0.85PMN-0.15KBT, (b) 0.75PMN-0.25KBT, and (c) 0.65PMN-0.35KBT compositions at different temperatures.

TABLE 1: Permittivity (ε) and capacitance (C) of $(1-x)$ PMN-(x) KBT at various temperatures.

Composition (x)	T (°C)	Permittivity (ε)	C (pF)
0.15	400	103.95	13.79
	450	107.72	14.20
	500	112.24	14.92
0.25	400	114.50	15.15
	450	146.89	19.70
	500	158.19	21.20
0.35	400	163.46	21.59
	450	189.83	25.31
	500	203.38	27.12

The imaginary modulus (M'') versus real modulus (M') plot at different measuring temperatures is shown in Figure 3. The intercept of the circular arc on the real axis (M') of M'' versus M' plot gives C_o/C_g, which means the inverse of the intercept of circular on the real axis gives the permittivity value. The arc corresponding to the grain boundaries has been suppressed and only one arc corresponding to the grains is seen in this sample. The C_g values were estimated from these graphs and the data are given in Table 1. The magnitude of grain capacitance increases with an increase in temperature and only the grain capacitance contribution is observed.

As it is seen, there is a shift of the intercept of the grain semicircle on the M' axis as the measuring temperature increase which implies the increase in capacitance. Here, being bulk capacitance (C_b) is inversely proportional to bulk resistance it shows the negative temperature coefficient of resistance of the material. The peak observed is expected to be due to relaxation in the grain component. Generally, the observed single semicircle from the M'' versus M' plots suggests grains contribution is leading. The implication is that the modulus plot highlights the smallest capacitance and the impedance plot highlights the largest resistance.

5. Conclusion

Investigation on the complex electric modulus of $PbMg_{1/3}Nb_{2/3}O_3$-$K_{1/2}Bi_{1/2}TiO_3$ electro ceramic properties was

reported in this work. The negative temperature coefficient of resistance behavior type is exhibited by $(1-x)$ PMN-(x) KBT electro ceramic compounds. Clearly, the presence of grain contributions has been shown by complex electric modulus plots. Important information about the relaxation processes of grain has been provided by the analysis of the complex electric modulus.

Data Availability

The authors confirm that the data supporting the findings of this study are available within the article. This is the experimental work. We are not using data from other sources.

Conflicts of Interest

The authors declare that they have no conflicts of interest.

Acknowledgments

The authors are thankful to the Research and Technology Transfer Centre, Wollega University, Nekemte, Ethiopia, and Department of Physics, University of Osmania, Hyderabad, India, for providing the necessary facilities to complete this work.

References

[1] S. Hajra, V. Purohit, M. Sahu, and R. N. P. Choudhary, "Electrical characteristics and conduction mechanism of microwave-sintered (Ba0.8Sr0.2)(Zr0.1Ti0.8Ce0.1)O3 electronic ceramics," *Indian Journal of Physics*, vol. 94, no. 2, pp. 175–182, 2020.

[2] A. Sridhar and M. A. Keip, "A phase-field model for anisotropic brittle fracturing of piezoelectric ceramics," *International Journal of Fracture*, vol. 220, p. 221, 2019.

[3] S. Mitra and A. R. Kulkarni, "Dielectric relaxation and electrical conductivity studies in $(100-x)$(Li0.12Na0.88)NbO3–xBaTiO3 $(0 \le x \le 40)$ ferroelectric ceramics: an impedance spectroscopic analysis," *Journal of Materials Science: Materials in Electronics*, vol. 31, no. 1, pp. 298–309, 2020.

[4] D. S. Saini, S. Tripathy, A. Kumar, S. K. Sharma, A. Ghosh, and D. Bhattacharya, "Impedance and modulus spectroscopic analysis of single phase BaZrO3 ceramics for SOFC application," *Ionics*, vol. 24, no. 4, pp. 1161–1171, 2018.

[5] T. N. Ghosh, A. K. Bhunia, S. S. Pradhan, and S. K. Sarkar, "Electric modulus approach to the analysis of electric relaxation and magnetodielectric effect in reduced graphene oxide–poly(vinyl alcohol) nanocomposite," *Journal of Materials Science: Materials in Electronics*, vol. 31, no. 18, 2020.

[6] S. B. Aziz, "Study of electrical percolation phenomenon from the dielectric and electric modulus analysis," *Bulletin of Materials Science*, vol. 38, no. 6, pp. 1597–1602, 2015.

[7] L. G. Wang, G. B. Yu, C. M. Zhu, F. Z. Lv, F. C. Liu, and W. J. Kong, "Preparation and investigation of structure, magnetic, and dielectric properties of $(1-x)$ Bi2Fe4O9-xMgFe2O4 bicomponent ceramics," *Journal of Materials Science: Materials in Electronics*, vol. 30, no. 23, pp. 20556–20565, 2019.

[8] A. V. Pushkarev, N. M. Olekhnovich, and Y. V. Radyush, "Dielectric properties of perovskite ceramics of $(1-x)$ BiFeO3–x(KBi)1/2TiO3 (0.40)," *Physics of the Solid State*, vol. 53, no. 3, pp. 522–526, 2011.

[9] S. Bag, P. Das, and B. Behera, "AC impedance spectroscopy and conductivity studies of Dy doped $Bi_4V_2O_{11}$ ceramics," *Journal of Theoretical and Applied Physics*, vol. 11, no. 1, pp. 13–25, 2017.

[10] M. H. Khan, S. Pal, and E. Bose, "Frequency-dependent dielectric permittivity and electric modulus studies and an empirical scaling in $(100-x)$BaTiO3/(x)La0.7Ca0.3MnO3 composites," *Applied Physics A*, vol. 118, no. 3, pp. 907–912, 2015.

[11] R.-Y. Jing, X.-M. Chen, J.-P. Ma, H.-L. Lian, and W.-T. Chen, "Synthesis, microstructure, and electrical behavior of (Na0.5Bi0.5)0.94Ba0.06TiO3 piezoelectric ceramics via a citric acid sol-gel method," *Journal of Materials Science*, vol. 53, no. 1, pp. 274–284, 2018.

[12] R. Das and R. N. P. Choudhary, "Dielectric relaxation and magneto-electric characteristics of lead-free double perovskite: Sm2NiMnO6," *Journal of Advanced Ceramics*, vol. 8, no. 2, pp. 174–185, 2019.

[13] M. N. Palatnikov, O. B. Shcherbina, V. V. Efremov, N. V. Sidorov, and A. N. Salak, "Microstructure and elastic modulus of ceramic Li x Na1−x NbO3 perovskite solid solutions prepared at 6 GPa," *Inorganic Materials*, vol. 46, pp. 1348–1352, 2010.

[14] F. Rehman, J. B. Li, Y. Saeed, and P. Ahmad, "Dielectric behaviors and electrical properties of Gd-doped Aurivillius KBi4Ti4O15 ceramics," *Journal of Materials Science: Materials in Electronics*, vol. 31, no. 1, 2020.

[15] N. A. Halim, W. H. A. Majid, and T. S. Velayutham, "Ferroelectric, pyroelectric and piezoelectric properties of CeO2-doped Na0.5Bi0.5TiO3 ceramics," *SN Applied Sciences*, vol. 1, no. 6, p. 582, 2019.

[16] M. N. Palatnikov, O. B. Shcherbina, V. V. Efremov, S. M. Masloboeva, S. V. Vladimirova, and D. V. Ivanenko, "Synthesis and comparative study of the microstructure and properties of $LiNbO_3$ and $LiNbO_3$:Zn ceramics manufactured by sol-gel processes," *Russian Journal of Inorganic Chemistry*, vol. 64, no. 5, pp. 673–679, 2019.

[17] Y. Wang, Y. Pu, Z. Wang, X. Li, and Y. Cui, "Dielectric, modulus and impedance analysis of (Ba0.9Bi0.1)(Ti0.9Al0.1)O3 ceramics," *Journal of Materials Science: Materials in Electronics*, vol. 28, no. 5, pp. 4245–4252, 2017.

[18] R. Kumar, M. Zulfequar, and T. D. Senguttuvan, "Improved giant dielectric properties in microwave flash combustion derived and microwave sintered CaCu3Ti4O12 ceramics," *Journal of Electroceramics*, vol. 42, no. 2, pp. 41–46, 2019.

[19] X. Hu, S. Rajput, S. Parida et al., "Electrostrain Enhancement at Tricritical Point for BaTi1−xHfxO3 Ceramics," *Journal of Materials Engineering and Performance*, vol. 29, 2020.

[20] C. Wang, T. Xia, X. Lou, and S. Tian, "Giant strain response in 2 mol% Nb-doped (Bi0.5Na0.4K0.1)TiO3 lead-free ceramics," *Journal of Materials Science*, vol. 52, pp. 11337–11345, 2017.

[21] S. F. Chérif, A. Chérif, W. Dridi, and M. F. Zid, "Ac conductivity, electric modulus analysis, dielectric behavior and Bond Valence Sum analysis of Na3Nb4As3O19 compound," *Arabian Journal of Chemistry*, vol. 13, p. 5627, 2020.

[22] S. Nasrin, S. M. Khan, M. A. Matin, M. N. I. Khan, A. K. M. Akther Hossain, and M. D. Rahaman, "Synthesis and deciphering the effects of sintering temperature on structural, elastic, dielectric, electric and magnetic properties of magnetic Ni0.25Cu0.13Zn0.62Fe2O4 ceramics," *Journal of Materials Science: Materials in Electronics*, vol. 30, no. 11, pp. 10722–10741, 2019.

[23] D. K. Mahato, A. Dutta, and T. P. Sinha, "Synthesis and electric characterization of rare earth double perovskite

Ho2CdZrO6 ceramics," *Journal of Electroceramics*, vol. 29, no. 2, pp. 99–105, 2012.

[24] B.-E. Jun, B. C. Choi, J. H. Jeong, and B. K. Moon, "Diffused phase transition of Ba1−x Eu x TiO3 ceramics," *Journal of the Korean Physical Society*, vol. 68, no. 12, pp. 1415–1419, 2016.